Magnetotelluric imaging of a Palaeozoic Andean margin subduction zone in western Victoria

Thesis submitted in accordance with the requirements of the University of Adelaide for an Honours Degree in Geophysics.

Michael Stepan

November 2014

THE UNIVERSITY of ADELAIDE

ABSTRACT

The geological setting for the accretion of the Lachlan and Delamerian Orogens in south-eastern Australia is controversial, with two different models proposed. The Lachlan Orogen resulted from either subducting oceanic crust and wedge accretion, or shortening and compression between two continental blocks. Broadband magnetotelluric (MT) data recorded over the transition between the Delamerian and Lachlan Orogens impose new constraints on the formation of southeastern Australia. The east-west MT survey extended for approximately 120 km, recording at 44 stations. A 2D inversion of the data in the bandwidth of 0.05-2000 s yielded a resistivity model to a depth of 150 km, with resistivity ranging from 1-10 000 Ωm. The upper crust was most resistive (>10 000 Ωm), and transitioned to a relatively flat conductor of 50-100 Ωm at ∼20 km. The upper mantle is resistive (>1 000 Ωm) and uniform below this layer. The Escondida, Moyston and Avoca Faults are imaged as low resistivity pathways (100-200 Ωm) extending to the surface. Faults may be anomalously conductive from alteration to serpentinite, and other trace mineralisation such as graphite. The Lachlan Orogen likely formed from west dipping subduction of mafic to ultramafic oceanic crust. This crust was altered to serpentinite, with magnetite coating grain boundaries. Imaged conductive bodies show where shearing caused interconnectivity of the magnetite.

KEYWORDS

Tasmanides, magnetotellurics, western Victoria, subduction

Table of Contents

List of Figures

INTRODUCTION

Eastern Australia is comprised of the Tasmanides, a series of orogens containing the Delamerian Orogen and Lachlan Orogen (VandenBerg, 1976; Foster & Gray, 2000; VandenBerg et al., 2000; Cayley, 2011). The Delamerian and Lachlan Orogens are Cambrian and Devonian aged respectively, and form western Victoria. The Lachlan Orogen can be further subdivided into the Benambran, Bindian and Tabberabberan Orogens (Cayley, 2011). Deformation was continuous from the Cambrian to Devonian, and named orogens correspond to periods of significantly increased rates of shortening (Cayley, 2011; Cayley et al., 2011). The Lachlan and Delamerian Orogens host world class orogenic gold belts, and related interconnected permeable networks that allow fluid to move from a deep source up through the crust.

Both the formation of the Lachlan Orogen and nature of the boundary between orogens is debated; two dominant models of orogenesis exist (Miller et al., 2005). The competing models are either orogenesis due to subduction, where the Lachlan Orogen formed as an accretionary wedge (Foster & Gray, 2000; Cayley, 2011), or intraplate orogenesis from colliding continental blocks, with crustal thickening and deformation (Rawlinson et al., 2010; Cayley et al., 2011).

Magnetotellurics (MT) is a passive geophysical technique which uses the Earth's electric and magnetic fields to image electrical resistivity (Chave & Jones, 2012). Resistivity is dependant on both fluid history and crustal composition, as both introduce conductive heterogeneities. Changes to crustal composition cause regional resistivity changes, whereas fluids are constrained to segregated channels and hence cause local anomalies (Simpson & Bahr, 2005).

MT may be used to image both ancient and active subduction zones at continental margins (Jones, 1993; Unsworth, 2010). Continent margins introduce resistivity variations by either fluid flow, melt, or mineralisation and alteration. Within ancient subduction zones, anomalies are due to mineralisation and interconnectivity of conductive minerals, particularly serpentinite (Reynard et al., 2011). Subducted mafic to ultramafic basalts associated with oceanic crust may be altered to serpentinite, with magnetite forming on grain boundaries (Stesky & Brace, 1973). Magnetite interconnectivity affects resistivity more than the percentage of magnetite (Parasnis, 1956; Kawano et al., 2012).

In this study, we deployed broadband (0.02-2000 s) MT instruments at 44 sites in an E-W transect, with a spacing of 3 km for the eastern 28 sites, reduced to 1.5 km for the remaining 16. This survey infills the data gap between surveys by Robertson et al. (2014) and Dennis et al. (2011b), creating a ∼400 km MT transect to complement the ∼500 km of seismic data. The intention of this study was to cross and image the transition between orogens, delineating history of the Lachlan Orogen. Integrating the MT inversion with previously collected seismic reflections, gravity and total magnetic intensity maps provides supplementary information not obtainable from MT alone. Defining major tectonic crust and resistivity structures constrains crustal evolution. New models can be used to better target gold and porphyry deposits in orogenic belts.

GEOLOGICAL SETTING AND BACKGROUND

Eastern Australia hosts a series of orogens, collectively known as the Tasmanides, shown in Figure 1 (Foster & Gray, 2000). The Delamerian and Lachlan Orogens are Cambrian to Devonian fold belts in western Victoria and South Australia. The Delamerian is the oldest orogen within the Tasmanides, active from about 520 to 490 Ma. The orogens

progressively young to the east, moving into the Benambran (455-440 Ma), Bindian (420 Ma) and Tabberabberan (390 Ma), all of which constitute the Lachlan Orogen (Cayley, 2011).

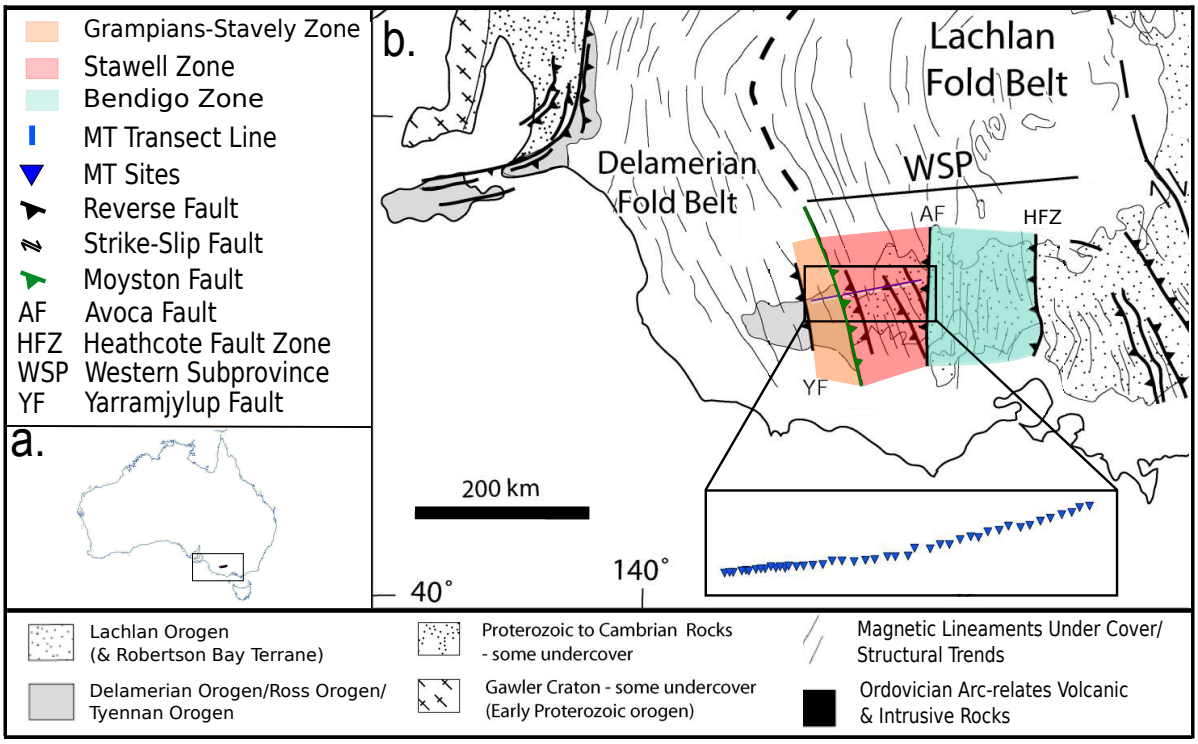

Figure 1: (a) A map of Australia showing the field area and 2014 MT line. (b) A location map of Victoria highlighting the terranes within the eastern Delamerian Orogen and western Lachlan Orogen. The 2014 MT transect line is shown striking ENE. The Moyston Fault is highlighted as it is a significant structure, potentially marking the boundary between the Lachlan and Delamerian Orogens. Terranes within orogens are also highlighted. Modified from Miller et al. (2005).

Deformation in the Ordovician was continuous and initiated with the Benambran Orogen, migrated east with time and terminated at the Tabberabberan; named orogens are periods of significantly increased rates of shortening (Cayley, 2011; Cayley et al., 2011). Metamorphic grade varies between the Lachlan and Delamerian Orogens, generally with a higher grade in the Delamerian, and particularly high grade at the transition between orogens (Cayley et al., 2011). The end of the Delamerian also marked the end of much

of the metamorphism (Foden et al., 2006). The eastern Lachlan Orogen hosts amphibolite facies metamorphism, with highest grade to the east, near the transition. Lower grade greenschist facies metamorphism is hosted in the Lachlan, grade again decreases to the east (Spaggiari et al., 2002; Foden et al., 2006). Blueschist facies metamorphism is observed in mélange within the Heathcote Fault Zone and elsewhere in the Tasmanides, indicating the high pressure low temperature environments common at subduction zones (Cayley, 2011; Foster & Gray, 2000; Spaggiari et al., 2002). The Moornambool Metamorphic Complex, the highest metamorphic grade rocks locally within the Lachlan Orogen were exhumed early in orogenesis, and is bound between the Moyston and Coongee Faults. (VandenBerg et al., 2000; Korsch et al., 2002; Cayley, 2011).

The Lachlan Orogen hosts world-class mineral and gold deposits which have been mined for over 160 years, to continue production new deposits must be discovered. Deeper exploration techniques are increasingly employed to search for conductive anomalies and fluid pathways related to mineralisation (Smith & Frankcombe, 2006). Faults are often utilised as fluid pathways, especially large scale faults that extend to the lithosphere and relate to gold mineralisation (Griffin et al., 2008; Willman et al., 2010; Griffin et al., 2013). The MT transect was conducted over the Grampians-Stavely Zone. The Stawell Zone is bound between the Moyston and Avoca Faults, and comprises the majority of the MT transect, it is richest source of gold within the Lachlan Orogen.

Illustrated in Figure 2, southeastern Australia has undergone history of extension and compression. Compression event shown in Figure 2b corresponds to the Lachlan Orogen. extension and subsequent compression resulted in exhumation of oceanic crust, followed by imbrication of this crust, and andesitic volcanism during compression and related subduction.

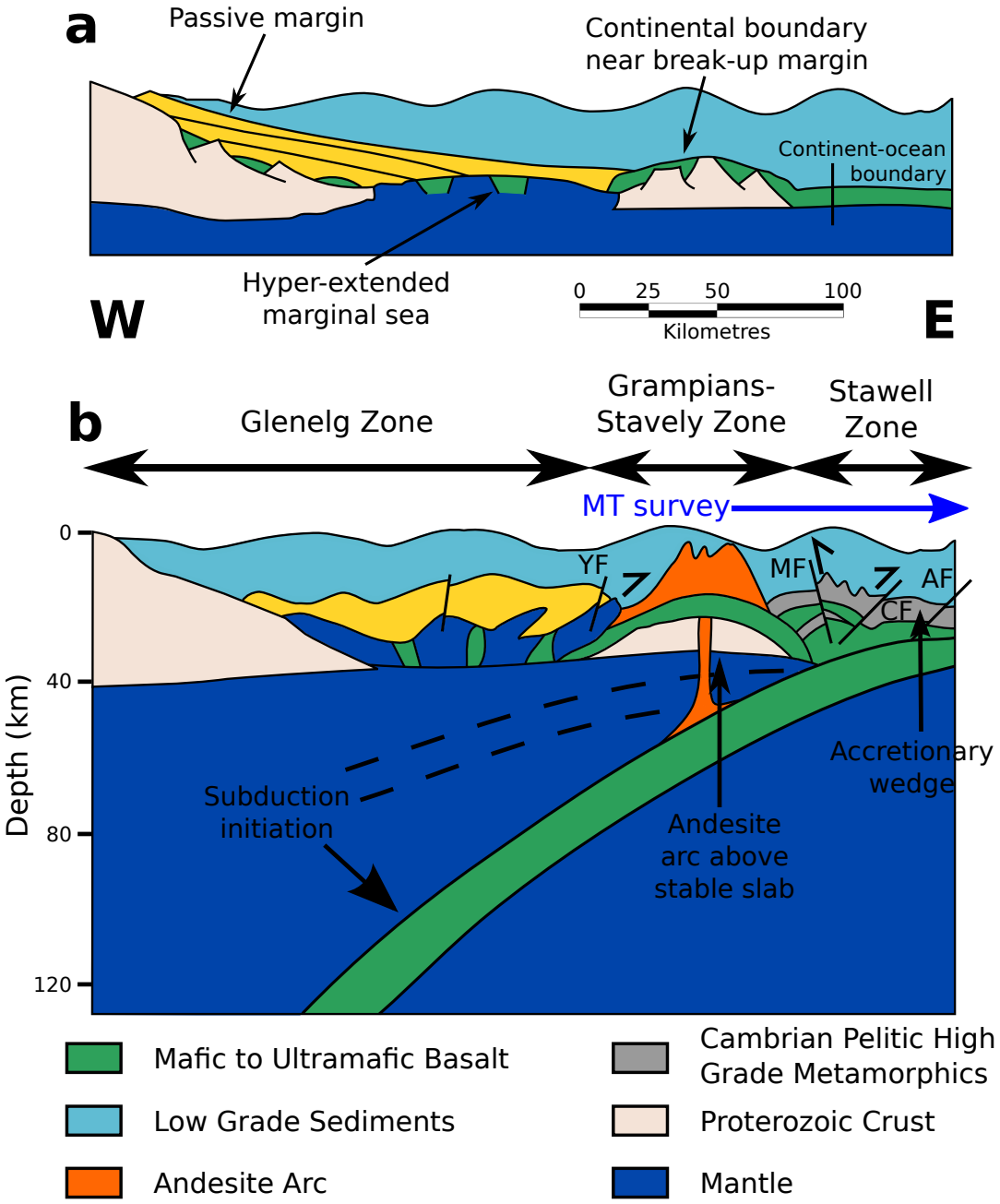

Figure 2: A model of compressional and extensional history of southeastern Australia. (a) Extension at ∼520 Ma of a passive margin. (b) Transition to compression at ∼500 Ma. Slab rollback due to extension has started. The Lachlan Orogen is forming to the east as an accretionary wedge, and emplacement of mafic wedges beneath the Grampians-Stavely Zone has begun. Compression continued for the next ∼80 Ma. Modified from Robertson et al. (2014).

Models of orogenesis

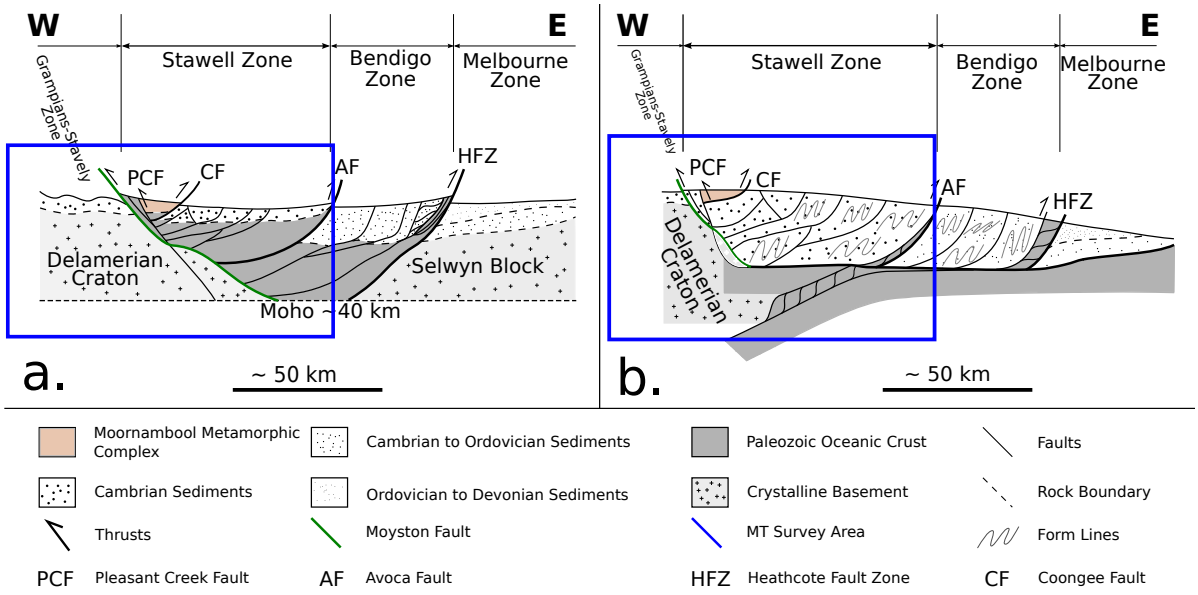

Figure 3: Two models for formation of the Lachlan Orogen. (a) The Selwyn Block or intraplate continent collision model of orogenesis. An external driving force caused orogenesis, with the Lachlan Orogen forming between the Selwyn Block and Delamerian Craton. Shortening was accommodated by synthetic and antithetic listric reverse faults. Ribbons of Paleozoic mafic to ultramafic oceanic crust were exhumed. (b) The subduction model of orogenesis. West dipping oceanic crust is subducted at a very low angle (Andean style subduction) beneath the Delamerian Craton. The Lachlan Orogen formed as an accretionary wedge above the subducting slab. Erosion and sedimentation results in the system younging to the east. The blue box shows where the MT survey location, but is not indicative of the depth imaged. Modified from Miller et al. (2005) with structural information taken from the seismic interpretation by Cayley et al. (2011).

The cause and style of orogenesis is still debated, with two dominant, competing models existing, juxtaposed in Figure 3. Figure 3a shows the model of intraplate deformation and orogenesis through continent-continent collision. This model has the Delamerian Orogen due to a subduction zone, and the Lachlan Orogen from a continent-continent collision and fault reactivation (Miller et al., 2005; Cayley, 2011). The Selwyn Block buttresses the Stawell and Bendigo Zones from the east, and no oceanic crust was subducted during the Lachlan. Shortening was accommodated by reverse faults and crustal

thickening (Foster & Gray, 2000; Cayley, 2011; Cayley et al., 2011). Highly conductive Murray Basin Sediments cover much of both orogens, typically obscuring geophysical responses; this is independent of the model of orogenesis (Smith & Frankcombe, 2006).

A competing model, Figure 3b has orogenesis due to subduction in the Ordovician, and is termed the subduction-accretion model (Miller et al., 2005; Cayley, 2011). This model proposes shortening by subduction of oceanic crust and the closure of an ocean. Subduction was likely low angle, explaining the lack of a coeval magmatic arc (Foster & Gray, 2000; Cayley, 2011). Thickening resulted from both sedimentary accretion as a wedge, and emplacing mafic wedges above Proterozoic crust. Slab rollback during the Cambrian lead to extension and formation of a back-arc basin, changing the environment from compressional to extensional, before further compression and the Lachlan Orogen (Soesoo et al., 1997; Fergusson, 2003; Foster et al., 2005; Fergusson, 2010). Potentially, more than one subduction zone exists for model 3b, occurring at different ages. Oceanic material is exhumed at the surface, so subduction must have occurred at some point during either the Lachlan or Delamerian Orogen (Spaggiari et al., 2003; Spaggiari et al., 2004). Up to four subduction zones within the Lachlan and Delamerian Orogens have been argued; this is outside the scope of this paper (Squire & Miller, 2003; Spaggiari et al., 2003; Cayley et al., 2011).

Both models interpret the Moyston Fault as the boundary between the Lachlan and Delamerian Orogens, however this may not be correct (Rawlinson et al., 2010; Cayley et al., 2011). No exact boundary may exist between the orogens, but rather a diffuse transition from one to the other.

MT response

Using MT to image the transition between the Lachlan and Delamerian Orogens may delineate the nature of orogenesis, and whether continent collision or subduction created the Lachlan Orogen. MT images electrical resistivity, and is more sensitive to conductive structures such as fluid filled faults and subducting mafic crust. Subduction zones are often anomalously conductive, this is attributed to fluid escape and dehydration in modern subduction zones, and mineralisation in ancient subduction zones (Jones, 1993; Worzewski et al., 2010). As the Lachlan Orogen may be the result of an ancient subduction zone, conductivity anomalies are attributed to mineralisation.

METHODS

MT methods

MT is a passive electromagnetic technique pioneered by Tikhonov (1950), and Cagniard (1953), which records natural variations in both the Earth's electric, **E**, and magnetic, **B**, fields. The magnetic and electric fields vary with time and are measured in two orthogonal directions on the plane of Earth's surface. A primary magnetic field induces a perpendicular electric field in the earth. For an Earth that varies resistively in two dimensions, the inductive field can be separated into two different modes, TE mode and TM mode. TE, or transverse electric, is defined by current flowing parallel to the geoelectric strike. TM, or transverse magnetic, describes perpendicular current flow (Simpson & Bahr, 2005).

Measured MT variations typically range from 10^{-3} to 10^{5} s. Periodicity is related to depth of investigation, with longer periods yielding greater depth of investigation. Depth of investigation, however, is also reliant on the resistivity, with a more conductive Earth

reducing depth of investigation (Simpson & Bahr, 2005). Shorter sounding periods (<1 s) are related to equatorial lightning and longer periods (>10 s) are due to ionising effects of solar winds (Chave & Jones, 2012). Between one and 10 s is a bandwidth of low signal strength, known as the dead band.

To relate the orthogonal electric and magnetic field components, the impedance tensor is used. The impedance tensor allows conversion between electric and magnetic fields, and is shown in (1). Impedance occurs when the fields pass through a conductive body, and the magnetic field induces an electric current. Delay exists between the magnetic field passing though a body and an electric field being induced. **E** is the electric field, **Z** is the impedance, which has both magnitude and phase, **H** is the magnetic permeability.

$$\begin{bmatrix} E_x \\ E_y \end{bmatrix} = \begin{bmatrix} Z_{xx} & Z_{xy} \\ Z_{yx} & Z_{yy} \end{bmatrix} \begin{bmatrix} H_x \\ H_y \end{bmatrix} \tag{1}$$

The phase tensor is a representation of the impedance tensor, free of galvanic distortion (Caldwell et al., 2004). Galvanic distortion is related to the scattered electric field, which is a result of the regional electric field being affected by local conductive heterogeneities. Generally, no distortion is assumed in the magnetic field (Bibby et al., 2005). The phase tensor, defined by (2), gives a ratio of the inverse of the imaginary part, $\mathbf{X^{-1}}$, to the real part, **Y**.

$$\Phi = X^{-1}Y \tag{2}$$

Phase tensor

The phase tensor can be graphically represented by an ellipse, where the maximum and minimum **Φ** values are the axes. Ellipticity of the function can be determined using (3).

$$\Phi = \begin{bmatrix} \phi_{xx} & \phi_{xy} \\ \phi_{yx} & \phi_{yy} \end{bmatrix} \tag{3}$$

These values give input to (4) which determines the ellipticity, and therefore dimensionality (Caldwell et al., 2004).

$$\epsilon = \frac{\phi_{max} - \phi_{min}}{\phi_{max} + \phi_{min}} \tag{4}$$

If the model has only one $\boldsymbol{\Phi}$ value or the $\boldsymbol{\epsilon}$ value is sufficiently small, the resulting ellipse will be regarded as a circle and therefore 1D. Larger $\boldsymbol{\epsilon}$ values result from 2D and 3D data and give an ellipse that is usually rotated and skewed, with the major axis oriented either towards or parallel to conductors (Caldwell et al., 2004).

Data acquisition

Measurements were collected using broadband MT coils and copper sulphate electrodes. Instruments recorded for 2-3 days at each of the 44 sites, with recording periods of 0.05-2000 s. The eastern 28 stations were spaced 3 km apart, whereas the western 16 stations had a 1.5 km spacing, for greater data density over the region of most interest. The location of the line was determined, in part, by seismic lines shown by Figure 4, to coincide with previously conducted surveys. Data were logged every five minutes, recording at 1000 Hz and decimated to 10 Hz to increase the period and depth of investigation. Dipole length was approximately 50 m in both north and east direction. Depth of investigation was defined by the skin depth, shown in (5), where $\boldsymbol{\delta}$ is skin depth in metres, $\boldsymbol{\rho}$ is apparent resistivity, and $\mathbf{T}$ is the period.

$$\delta = 500\sqrt{\rho T} \tag{5}$$

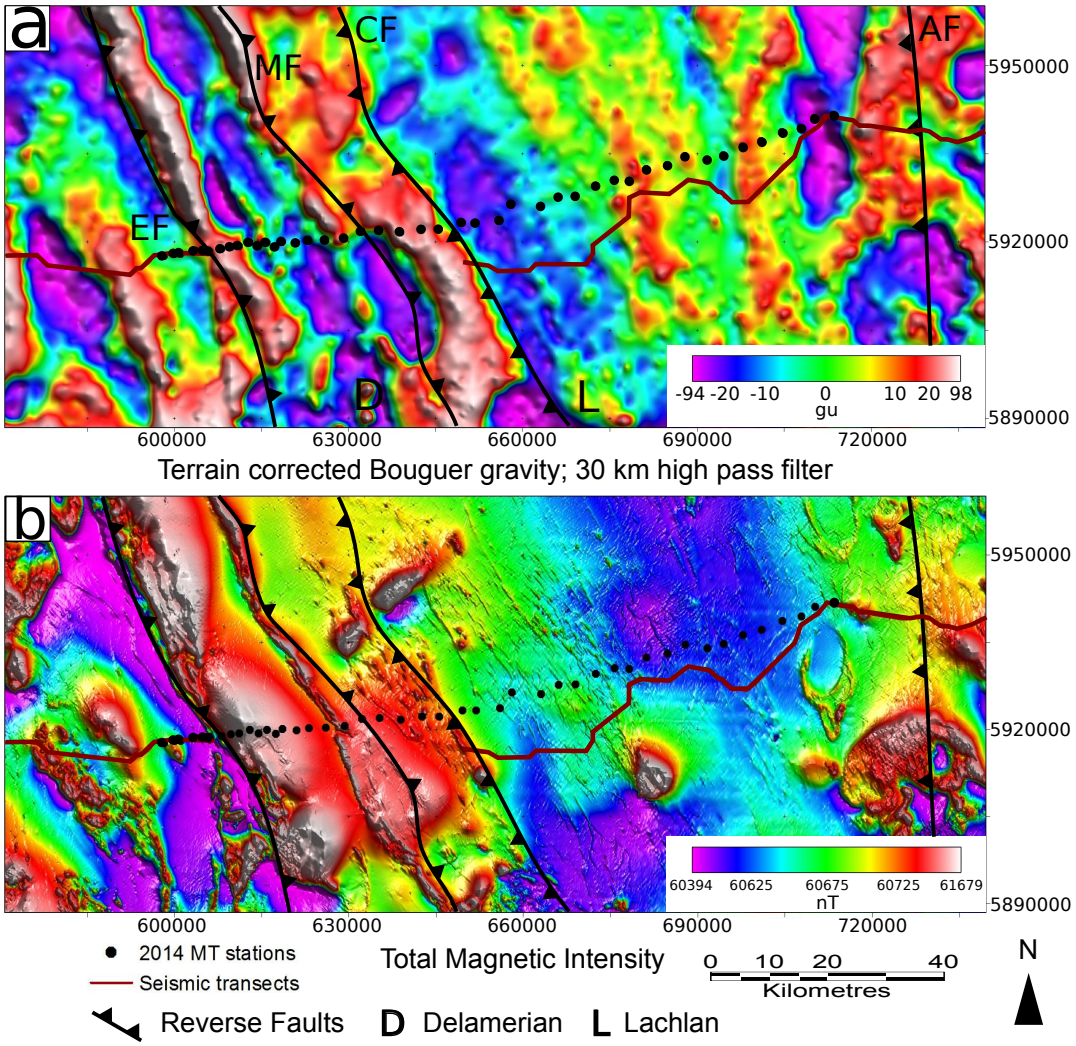

Figure 4: Geophysical maps of the study area, identifying MT sites and adjacent seismic lines. The same faults are interpreted on both maps, and whilst more faults are identifiable only major faults are interpreted. strike of major features and lineaments are sub-perpendicular to the transect (a) A gravity map with a high pass filter, making shorter wavelength (smaller) features visible. (b) A total magnetic intensity map, primarily identifying faults, but also showing magnetic lineaments. P. Skladzien pers. comm. 2014. (EF) Escondida Fault; (MF) Moyston Fault; (CF) Coongee Fault; (AF) Avoca Fault.

Skin depth for this survey, assuming 100 Ωm and 1000 s was ∼150 km.

Processing and pre-inversion

Data quality were assessed by eye, and the best interval of data were selected at each site. Fifty, 100, and 150 Hz notch filters were applied to remove common sources of noise. Processing was done using the BIRRP robust method, and utilised remote referencing of sites recording at simultaneous times to reduce errors associated with magnetic interference (Shalivahan & Bhattacharya, 2002; Chave & Thomson, 2004).

RESULTS

Data

A smooth 2D inversion using the nonlinear conjugate gradient method created the final model. Data from 40 of the 44 sites were used in the inversion. Four sites were omitted due to poor data quality, indicated in Figure 5. Final root mean square achieved was 3.4, where the target was one. Data errors for TE were 15% for the apparent resistivity, and 50% for phase. TM data errors were 5% and 2.5% respectively. The τ value was two, as a compromise between a smooth, geologically reasonable model, and a complex model to fit the data. Outliers in the data or points with erroneous phase were muted as they would adversely affect the inversion. The final model had a resistivity range of 1-10 000 Ωm.

Pseudo-sections presented in Figure 5 show the data quality for both modes, and offer a visual measure of lateral continuity. Sharp boundaries or inconsistencies indicate poor quality data, resulting in a poor quality inversion. Pseudo-sections are the data pre-inversion, so are unbiased by imposed conditions and assumptions. Trends of data may

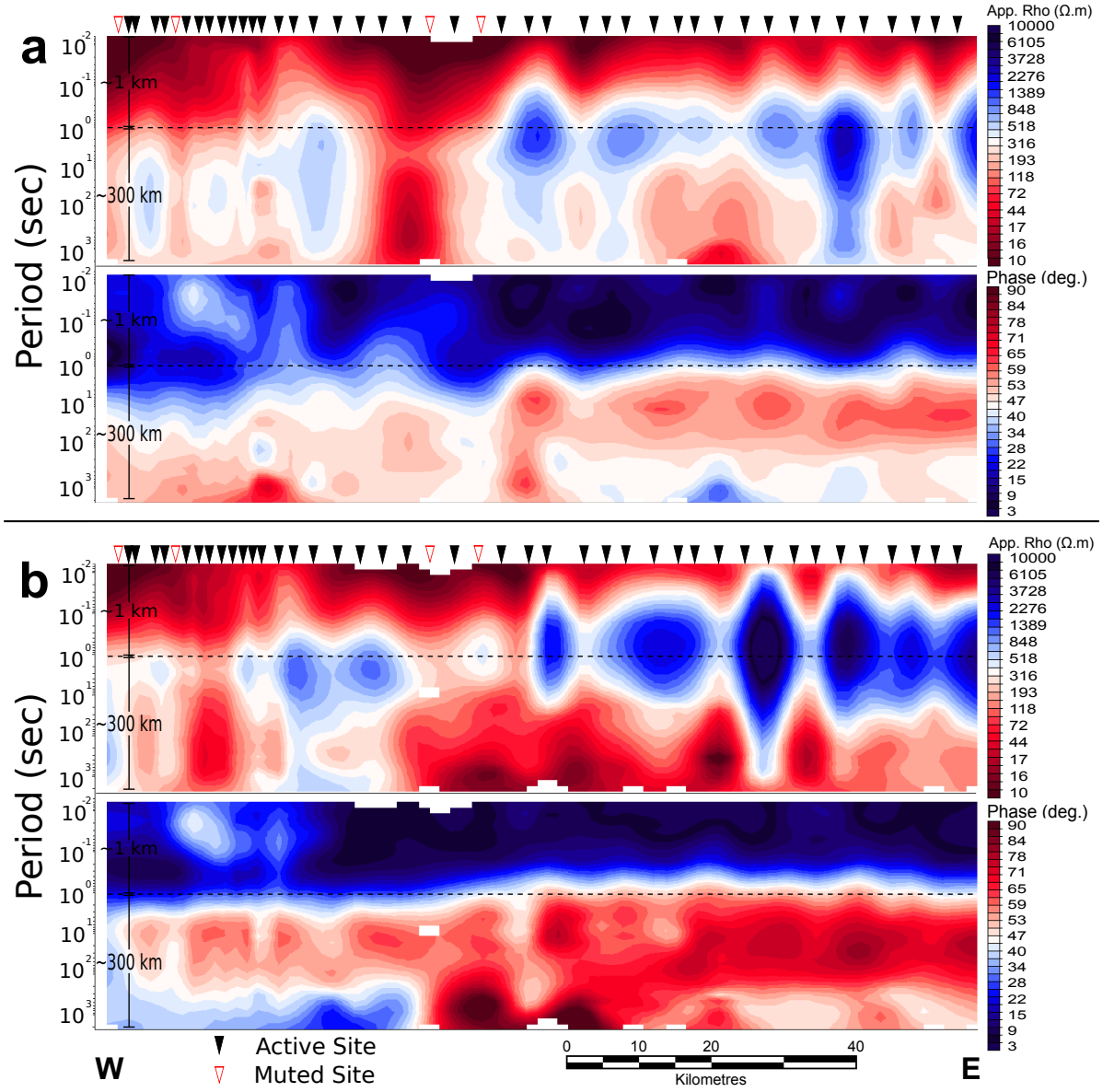

Figure 5: Pseudo-sections for TE (a) and TM (b) mode, showing both apparent resistivity and phase. Period is analogous to depth, where greater period corresponds to greater depth. The log period y-axis causes a deceptive scale, where above the dashed line (1 s) is ∼1 km, but below the dashed line is ∼300 km. Blank spaces in the sections indicate where the interpolation radius is less than the spacing between data points. Muted sites have no influence.

be estimated from the sections, but more importantly, erroneous sites can be identified and muted (Caglar, 2001). TE and TM mode are presented separately and give slightly different responses.

Figure 6 supports a 2D inversion of the data, as does Figure 4. Figure 6 shows variations primarily in depth, and Figure 4 shows consistent regional geological strike, which may approximate 2D. The final inversion of the data was a 2D model, as this was the most appropriate dimensionality. Data can therefore not be accurately modelled in 1D (Caldwell et al., 2004; Galanopoulos et al., 2005). Figure 6 shows how phase ellipses react to varying dimensionality, where less circular ellipses indicate 2D structure, with greatest contrast between modes (Thiel, 2008).

Phase and pseudo-sections

Pseudo-sections are shown in Figure 5. Warm and cool colours show some correlation between modes phase and apparent resistivity. Resistivity is high for <1 s, decreases from 1-50 s, and again increases for the longer periods (>50 s). Layering is only weak however, and somewhat segregated, rather than pervasive. Phase shows more defined layering than resistivity, with strong contrast and transition from low to high beneath one second. High phase beneath eastern sites at >1 s dips west, transitioning to a slightly lower ($>45^o$) phase angle beneath the western sites. Low phase indicates conductive bodies overlying resistive, and the opposite is true for high phase. Vertical log scale of Figure 5 provides an exaggerated scale at shallow depths, giving a more detailed image of the Murray Basin Sediments. Pseudo-sections cannot however be interpreted as models of the subsurface, and this is not their purpose.

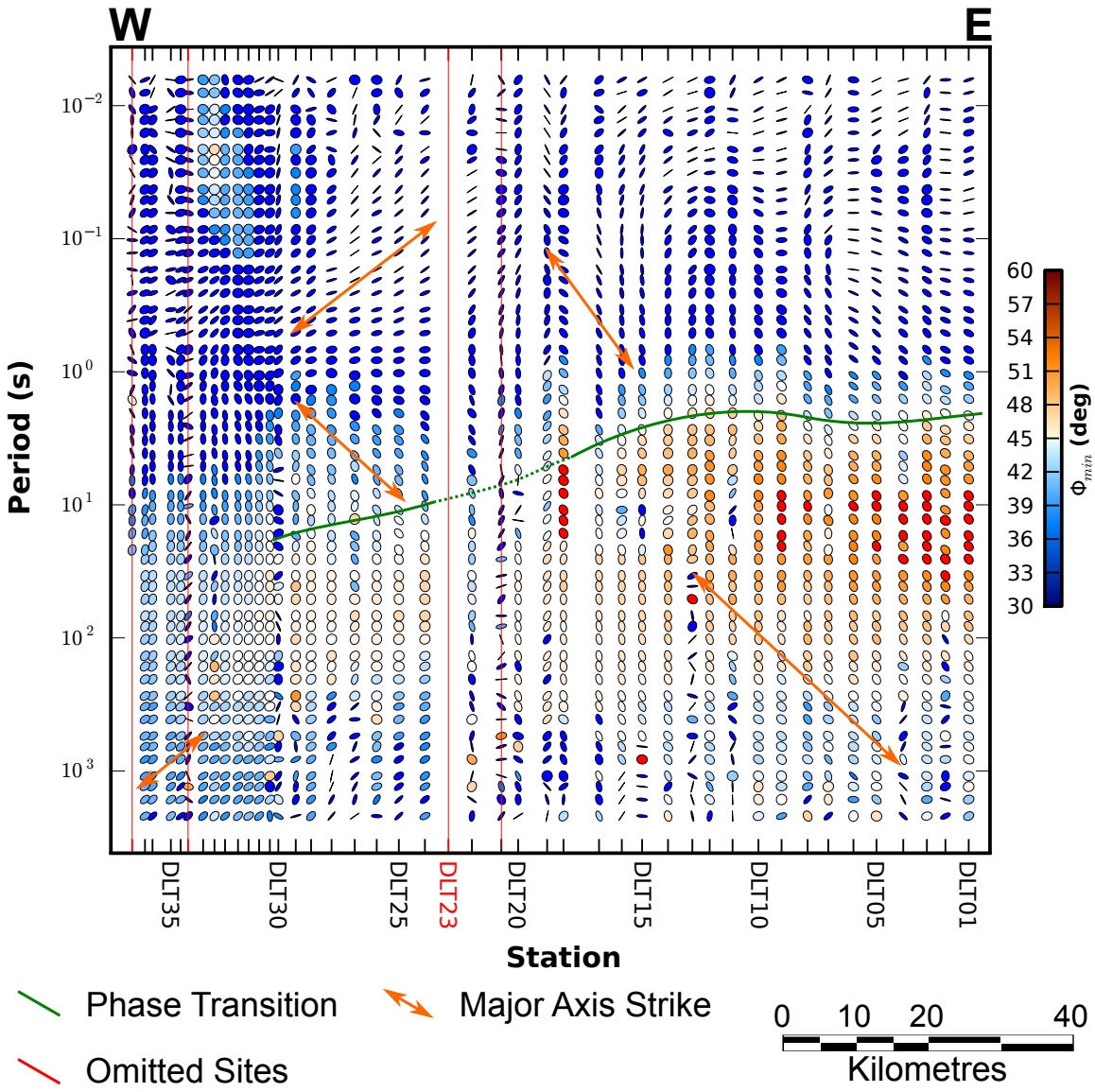

Figure 6: Phase ellipses at different periods and stations, along the MT line. Ellipticity shows dimensionality of the data, where elliptical points show either 2D or 3D structure. Minimum phase angle of ellipses indicate conductivity is decreasing with depth for up to ~2 s (cool colours), and increasing with depth for greater than ~2 s (warm colours). The green line indicates the approximate period at which the phase changes to greater than 45^o, indicating increasing conductivity with depth. Orange arrows are the predominant orientation of the major axes of surrounding ellipses, and either point towards, or are parallel to conductive bodies. As ellipse orientation provides a strike line, 180^o ambiguity of direction exists. Red sites are phase $<30^o$ or $>60^o$. Omitted sites were deemed too noisy to provide information, hence removed from the inversion. Phase ellipses at these sites cannot be used for interpretation. No processable data were collected at site DLT23. Inconsistent spacing of station numbers in the west is due to fill-in sites (e.g. DLT30a).

Within Figure 6, ellipses at site DLT21 are elongate with no preferred orientation, this is characteristic of noise. Sites DLT20 and DLT22 are also elongate and somewhat randomly oriented, but to a lesser degree than site DLT21. Consistent phase at different skin depth indicates the signal is caused by a geological source rather than random noise, sites at the west of the survey show a similar response. Figure 6 shows muted sites, but ambiguity exists as to whether the sites are noisy due to a geological source or instrument error. Orientation of ellipses can help determine this, shown by the orange arrows. The arrows show the trend of ellipses, which orient either towards, or parallel to conductive bodies. Ellipses adjacent to sites DLT21 orient towards it at >1 s, and ellipses west of site DLT23 orient away at ∼10 s.

Below the green line in Figure 6 is a westward deepening trend, where phase ellipses indicate increasing conductivity with depth and are nearly circular, approximating 1D; the same response is observed in Figure 5b. Short periods have a low phase angle, $<45^o$, denoting decreasing conductivity with depth, this changes abruptly at ∼1 s to $>45^o$. Depth of the phase change decreases suddenly west of site DLT20, suggesting displacement. Beneath these high phase regions data quality is generally reduced, showing the adverse effect of conductivity on depth of investigation.

2D inversion

Figure 7 shows two connected, moderately conductive layers exist at ∼20 km, which extend the length of the survey. They are slightly curved and both gradually dip away from the centre of the transect. Dip and depth of the conductors changes at the Moyston Fault, from ∼20 km deep at the east of the transect, to ∼25 km at the west. Dip also changes at the Moyston Fault, from west at ∼10° in the east, to east at ∼20° in the west. A third, slightly deeper sub-horizontal conductor (C4) is observed at the east

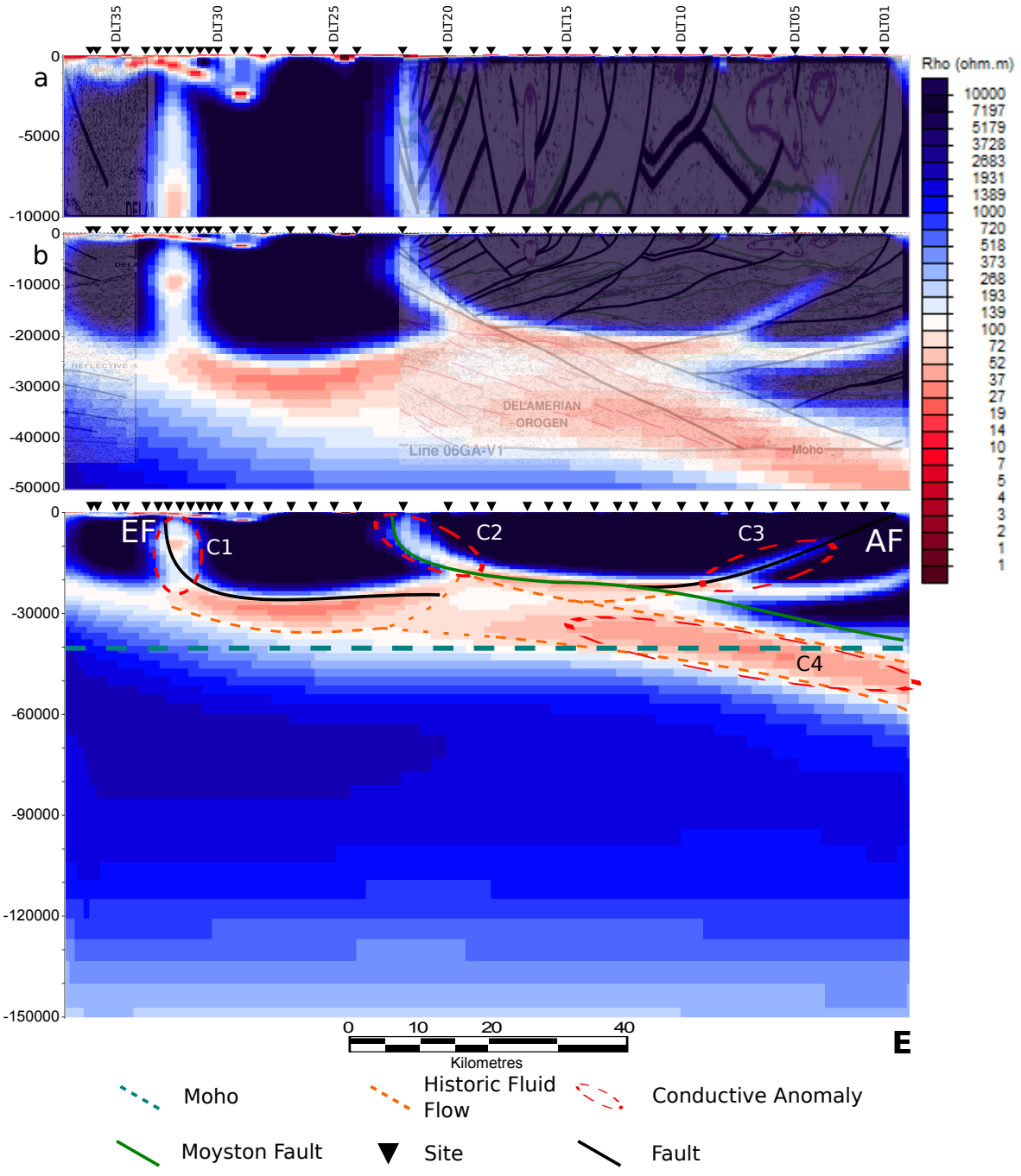

Figure 7: A 2D inversion of the MT data at three scales: from the surface to 10 km (a), 50 km (b) and 150 km (c). Seismic interpretations by Korsch et al. (2002) and Cayley et al. (2011) are overlain on (a) and (b). Structure, fluid pathways and conductors are interpreted in (c).

of the transect, dip is also to the east, and steeper than the other conductors. Three anomalously conductive, sub-vertical pathways branch off the two upper conductors. These pathways (C1, C2, C3) extend to the surface and have resistivities of 50-100 Ωm. Upper crustal resistivity is >10 000 Ωm. Fluids percolating upwards through the crust are known to fill connected fracture networks at ∼20 km, especially when related to subduction (Simpson & Bahr, 2005). Conductors in Figure 7 are unlikely to be imaging fluids, due to age of the system, but may be imaging mineralisation as a result of past fluids. Below conductors, the mantle has a uniform resistivity of ∼ 1 000 Ωm.

DISCUSSION

Ultimately, the 2D inversion is a model constrained by assumed parameters so does not show the true earth, but as said by George Box 'All models are wrong, but some are useful' (Box & Draper, 1987). The inversion itself is therefore not a stand alone answer to the subsurface, but should be supplemented with the raw data, or integrated with other geophysical methods.

Sub-vertical conductive pathways, C1, C2, and C3 in Figure 7 are interpreted as faults and branch off a décollement at a depth of ∼20 km; faults are both east and west dipping (Phillips et al., 2002; Willman et al., 2010). C1 is the Escondida Fault, C2 the Moyston Fault, and C3 is the Avoca Fault. All three faults formed during the Lachlan Orogen and separate significantly different units. The Moyston Fault is the largest of the three, the Escondida Fault joins it at depth, and the Avoca Fault is antithetic to and is truncated by the Moyston Fault. All three faults are reverse, and listric at ∼15 km.

Conductive anomalies can be attributed to either mineralisation, a fluid phase, or melt (Jones, 1993; Simpson & Bahr, 2005). Mineralisation and fluid phase both require

fluid flow. Resistivity of a fluid phase is dependant on salinity and volume of fluid, while resistivity of mineralisation or melt depends on composition (Hyndman & Shearer, 1989; Hyndman et al., 1993; Jones, 1993). Interconnectivity of the conductive phase also significantly effects resistivity (Parasnis, 1956). Two common types of mineralisation within ancient subduction zones are graphitic schists and serpentinisation (Jones, 1993; Unsworth, 2010; Worzewski et al., 2010).

Integrated geophysics

Other geophysical surveys have been conducted in the study area previously, some of which are shown in Figures 4 and 8. Geophysical surface maps of the area and seismic section provide additional information not obtainable from MT. Figure 4 presents gravity and total magnetic intensity (TMI) maps, while Figure 8 stitches together interpreted seismic sections. Major conductive pathways spanning from the mantle to the surface in Figure 7 correspond to interpreted faults in the seismic section, and sharp boundaries in the TMI and gravity maps.

Gravity and TMI maps in Figure 4 both identify major faults striking NNW. East of the Coongee Fault, zone L shows smooth, diffuse boundaries and low TMI response. West of the Coongee Fault, marked D, gravity and TMI maps are less smooth. Discrepancy either side of the Coongee Fault may be interpreted as marking a boundary between orogens, but the TMI and gravity highs can be attributed to the Moornambool Metamorphic Complex (VandenBerg et al., 2000; Crawford et al., 2003). Between the Escondida Fault and Moyston Fault in Figure 4, a distinct, ridge like feature with the same strike as the Moyston Fault is observed. This structure is the Mount Dryden Fault, it is not present in Figure 7, and does not significantly affect phase ellipses in Figure 9. The Mount Dryden Fault post-dates the Delamerian Orogen, and did not undergo

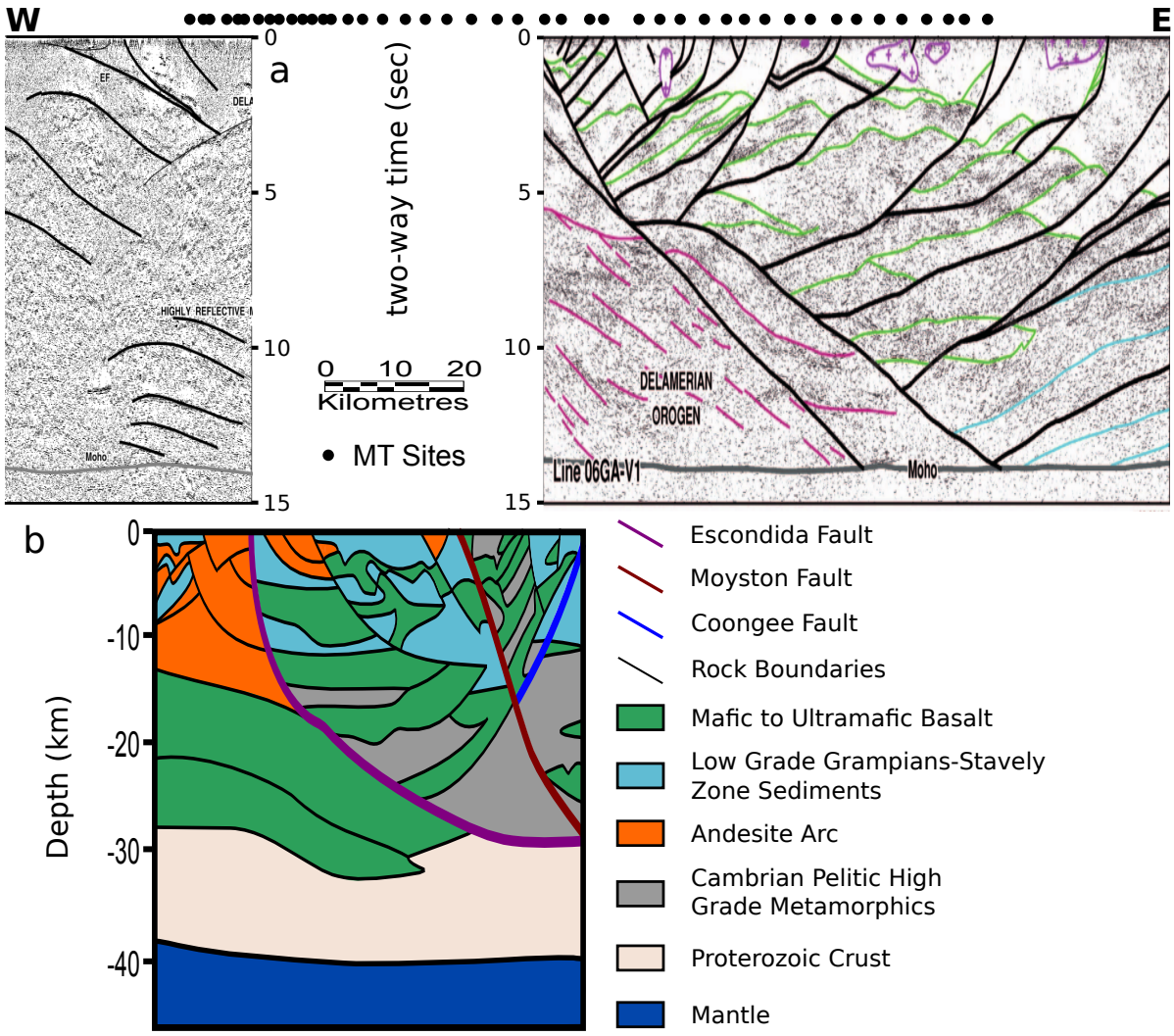

Figure 8: Interpreted seismic sections coincident with the MT line. The seismic lines do not exactly correlate to the MT line, but are close enough they may be used. (a) Structure, primarily faults, interpreted directly onto seismic sections. The gap between sections is the break in seismic lines is due to data being collected in different surveys. MT sites shown are from the 2014 line, not related to collecting the seismic data, they are included as reference points. Interpretations were by Cayley et al. (2011) and Korsch et al. (2002), assumed seismic velocity was 6 km/s. (b) A colour seismic interpretation. Coloured faults correspond to major faults in the area. Slivers of mafic to ultramafic basalt, potentially serpentinised, are exhumed between the Moyston and Coongee Faults Modified from Cayley et al. (2011a). The section fills the gap between sections in (a). Vertical exaggeration for both is 2:1.

subsequent conductive alteration.

Major structures in Figure 4 strike NNW, and influenced the east-west orientation of the transect. The TMI map contains more variation and complexity here than further north or south. Location of the survey was also dictated by previous MT surveys which are not shown, and seismic lines which are shown in Figure 8.

Overlaying phase ellipses on geophysical maps in Figure 9 provides an indication of how TMI and gravity relate to MT. Some structure may only be identifiable by collating data, such as by phase ellipses on TMI or gravity maps. Skin depth and geophysical technique were specifically paired. Ellipses from shorter period were overlain on a TMI map, as TMI is more affected by shallow features. Longer period ellipses however were overlain on the gravity map, as gravity is more influenced by longer wavelength structure.

Figure 9 shows both minimum phase angle and ellipticity change primarily at faults. East of the Coongee Fault, ellipses align to the regional geological strike. Being directly over such a large fault could explain the 3D response above the Moyston Fault in Figure 9a, and Coongee Fault in Figure 9c, as current channelling would be significant this close to a major conductive feature (Simpson & Bahr, 2005). East of the Coongee Fault, phase ellipses at 100 s are predominantly elliptical, whereas they are circular to the west. Current channelling due to faulting creates local 3D distortion for 2D resistivity structures, the field area east of the Coongee Fault is therefore potentially significantly faulted (Bahr, 1988; Caldwell et al., 2004; Bibby et al., 2005).

Between the Moyston and Escondida Faults minimum phase angle increases, the increase corresponds to a TMI high in Figure 9a. At 0.01 s, phase increases to almost 45^o

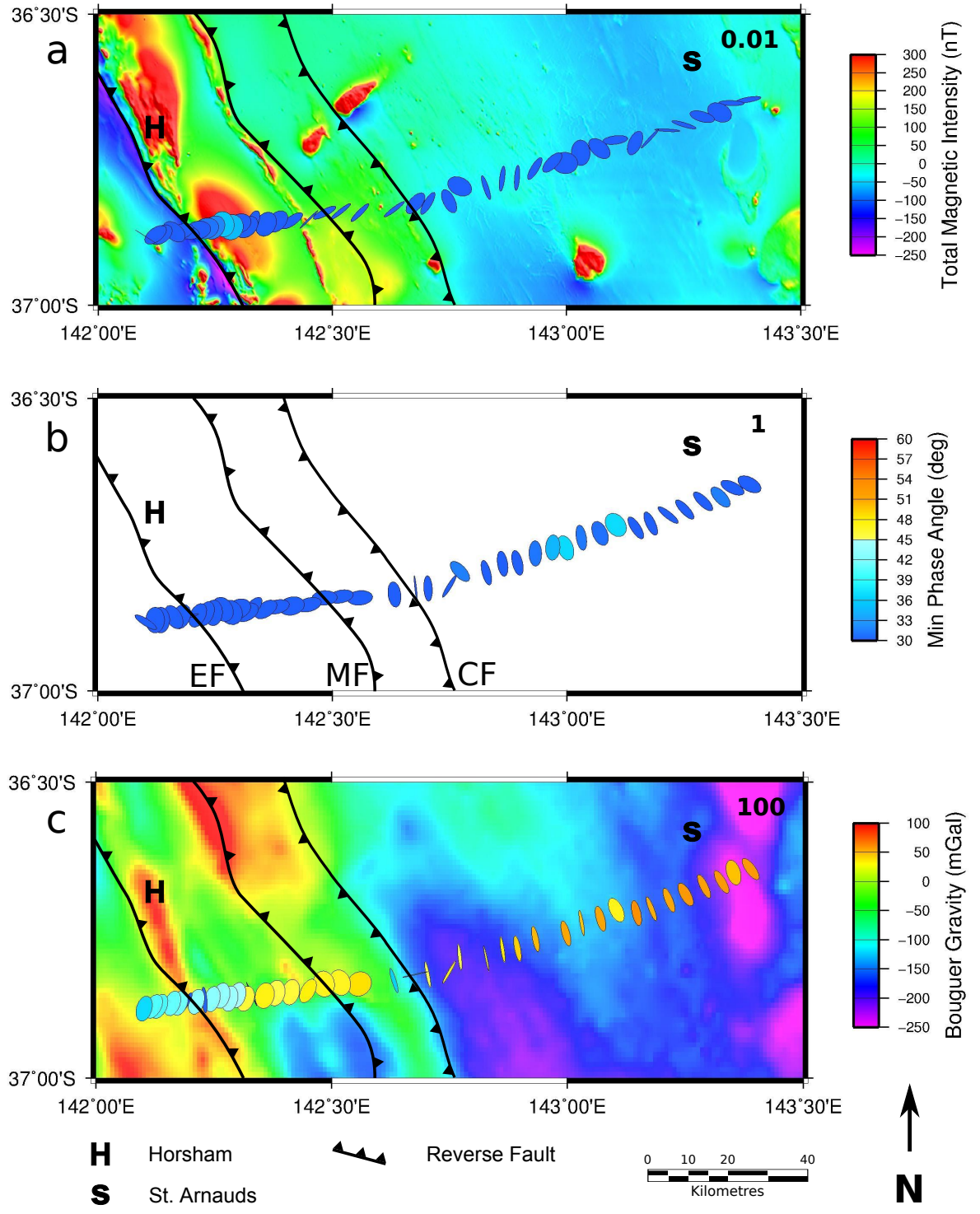

Figure 9: Phase ellipses at (a) 0.01, (b) 1 and (c) 100 s projected onto geophysical maps. Approximate skin depths are 0.5 km, 5 km and 50 km respectively. (a) is overlain on a TMI map, and (c) is overlain on a gravity map, with no filters applied. Minimum phase angle colour bar applies to phase ellipses for all three periods. Faults cause abrupt changes in minimum phase angle and dimensionality of ellipses, and can be used to determine fault locality. Interpreted faults are the same across the three maps.

for two sites, before returning to the value consistent with the other sites. At 100 s, just east of this anomaly phase changes to $>45^o$ for the remainder of the survey. Phase is circular at these sites across the three periods. Not all faults affect phase ellipses, the Escondida Fault, a major fault, shows no phase anomalies. Ellipses predominantly orient parallel to regional strike, with only some ellipses at 0.01 s aligning towards conductors. The weak alignment observed is not sufficient to infer structure or regional trends. Anomalous ellipses more clearly identify faults, but distinguishing between faulting and noise, without supplementary data such as surface maps, can be impossible.

Deep seismic surveys undertaken in the area show significantly different lithospheric responses transitioning from the Delamerian to Lachlan Orogen (Graeber et al., 2002; Rawlinson & Fishwick, 2011; Aivazpourporgou et al., 2013). Observed velocity changes are consistent with changing from continental to oceanic lithosphere (Cammarano et al., 2003; Faul & Jackson, 2005). Teleseismic surveys conducted by Rawlinson et al. (2010) show a high velocity feature east of the MT survey in the central part of the Lachlan Orogen, interpreted as competent crystalline crust, potentially the Selwyn Block.

The highest resolution geophysical surveys conducted in the area are the seismic surveys. Seismic data have been collected at different stages over the last 18 years, to almost completely cover the transition between orogens; the 2014 MT line follows these surveys. Seismic lines are presented in Figure 8 and interpretations by Korsch et al. (2002), Cayley et al. (2011) and Cayley et al. (2011a) aided in interpreting Figure 7.

Seismic interpretations in Figure 8 are higher resolution than MT, and show faulting in the upper crust. Faults do not need to have undergone conductive alteration to be visible in seismic sections, like they do in MT. Seismic surveys can however only image

as deep as the Moho, ∼40 km in the study area, much shallower than MT depth of investigation, which is more than 300 km. Resolving features in the lower crust aids in determining source of fluids.

Integrating MT inversions with seismic sections serves another important purpose, constraining depths to conductors and the Moho (Jones, 1987; Hyndman & Shearer, 1989). MT poorly constrains depths to conductors and structure beneath any crustal conductors (Jones, 1987). Seismic reflections impose depth control on MT, and have been used to some extent in Figure 7. C4 in Figure 7 cannot necessarily benefit from control from seismic data, as it potentially extends to below to Moho. As C4 may be a conduit for the upper conductive anomalies, whether this structure crosses the Moho or not determines if fluids were sourced from the mantle or crust.

Structure in Figure 7 agrees well with seismic interpretations, although scale and fault locations change slightly between the inversion and seismic interpretations (Korsch et al., 2002; Cayley et al., 2011). Importantly, the Moyston and Avoca Faults correlate closely between both the interpretation by Cayley (2011) and Figure 7, though trace at depth differs slightly. The seismic section interpretation is far more detailed than the MT inversion however, as faults interpretable in the seismic section are invisible in the inversion.

Conductive alteration is necessary for faults to be imaged and interpreted in MT, but not in seismic sections. Inability to identify interpreted faults in the inversion could therefore be due to a variety of reasons. Faults may be sufficiently small they are below the resolution of MT, and hence not imaged, faults of this scale are unlikely to be significant. MT is however very sensitive to conductive structure, so even small scale faults

should alter conductivity anomalies (Simpson & Bahr, 2005; Chave & Jones, 2012). The more likely reason for the faults not being modelled is they are not anomalously conductive. Faults would not be anomalously conductive if they did not contain an interconnected phase of conductive minerals, the source of conductance in Figure 7. Faults with no interconnected conductive anomalies will be invisible to MT, yet still interpretable in a seismic section. Between the Moyston and Avoca Faults in Figure 7a, small, slightly anomalous conductors ($\sim$300 Ωm) exist at the surface which correlate to faults interpreted by Cayley et al. (2011).

The actual path of the seismic line is shown in Figure 4, it does not exactly correspond to the MT line and neither does it have a constant strike. Data are not continuous across the survey, and the gaps, and later fill, are shown in Figure 8. Faults interpreted in the seismic section, but not MT section, may be oriented so they do not intersect the MT line, or are sufficiently far from the transect and too shallow to significantly affect resistivity. Consistent regional strike suggests faults likely intercept the MT transect, so not being imaged is a result of not undergoing conductive alteration.

Alteration of mafic and ultramafic oceanic crust

Horizontal conductors at 20-25 km are not exceptionally conductive, ranging from 50-100 Ωm. This is too resistive to be graphite, but within the bounds of what can result from a fluid phase, as Hyndman & Shearer (1989) and Hyndman et al. (1993) measured lower resistivity in rocks with $<$1% porosity. As deformation and subduction occurred $\sim$400 Ma, subduction related fluids are unlikely to cause the anomaly. Younger fluids, unrelated to orogenesis may give an anomalous response, although anomalies are likely still mineralisation (Jones, 1993). Modelled resistivity (50-100 Ωm) and observed outcrop in adjacent areas suggest the anomaly is serpentinisation of mafic and ultramafic

basalts (Stesky & Brace, 1973; Crawford et al., 2003; Myer et al., 2013). Ribbons of mafic to ultramafic oceanic crust have been exhumed both east and west of the MT line (Foster & Gray, 2000; Spaggiari et al., 2002). Serpentinite alone is unlikely to image such a low resistivity, the alteration pathway taken however produces magnetite, which can cause the observed resistivity (Reynard et al., 2011; Kawano et al., 2012).

Serpentinisation within the Lachlan and Delamerian Orogen altered the mafic and ultramafic basalts in Figure 8b (Crawford et al., 2003; Robertson et al., 2014). The serpentinisation and magnetite in Figure 8 is likely more extent than the resistivity anomaly in Figure 7, and more layered (less massive). Layered nature of the mafic to ultramafic slivers is not modelled, potentially due to MT poorly constraining the base of conductors (Jones, 1987; Hyndman & Shearer, 1989).

Mafic and ultramafic oceanic crust was sourced from Proterozoic crust exhumed during extension prior to the Delamerian Orogen (Foden et al., 2006). During the Lachlan Orogen, this mafic to ultramafic crust was compressed and exhumed (Crawford et al., 2003). Serpentinisation of the crust was widespread, and often resulted in magnetite along grain boundaries, causing anomalies. More important than the amount of magnetite is the interconnectivity (Reynard et al., 2011; Kawano et al., 2012; Myer et al., 2013; Ferguson et al., 2015). Figure 10 shows how for the same volume of magnetite, resistivity can differ by orders of magnitude. Conductive responses in Figure 7 are interpreted as regions of increased magnetite connectivity due to shearing (D. Taylor 2014 pers. comm., Kawano et al., 2012).

Conductors C1, C2 and C3 in Figure 7 are therefore anomalously conductive because of magnetite interconnectivity rather than composition. Shearing during the Escon-

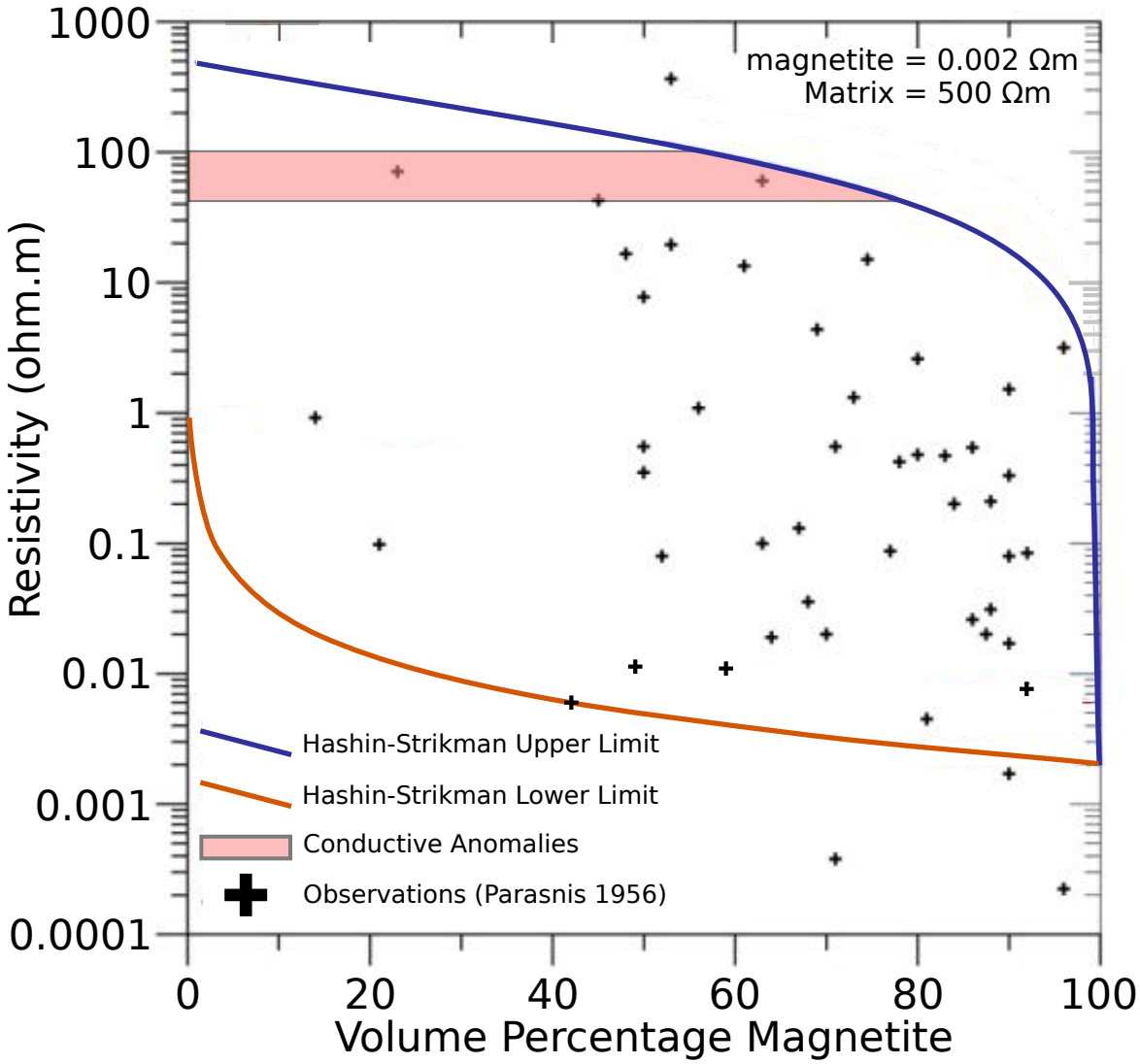

Figure 10: A plot of resistivity values against percentage of magnetite. Solid and dashed lines at the top and bottom of the plot constrain most of the points. Between the lines exist the volume percent of magnetite and corresponding resistivities which may co-exist. Conductivity variations are due to degree of magnetite interconnectivity. The red box correlates to the observed conductivities of anomalous bodies in this study. Modified from Ferguson et al. (2015).

dida, Moyston and Avoca Faults may have caused the magnetite around grain boundaries to deform and become interconnected, resulting in conductive pathways (Kawano et al., 2012; Myer et al., 2013). This mechanism explains the extent mafic to ultramafic serpentinised zones in Figure 8, yet segregated conductors in Figure 7. Fluids initially must have been present to allow serpentinisation, which lead to magnetite forming on grain boundaries (Stesky & Brace, 1973; Jones, 1993).

Fluids can be either mantle or crustally derived, and depends on whether C4 in Figure 7 is the conduit for fluids, and if it is truncated at the Moho. Seismic depth control of MT will help define this. Figure 8 shows the top of C4 is defined by the Moyston Fault, and the bottom is constrained by the Pleasant Creek Fault. MT depth control issues again arise here, where difficulty exists in defining C4 as either one thick conductor, or two thin conductors (Jones, 1987; Hyndman & Shearer, 1989). Both faults terminate abruptly at the Moho in the seismic section, but propagate through in the MT inversion.

Depth to C4 may also be influenced by edge effects. Edge effects can cause modelled conductors to divert from their actual path, potentially the case in Figure 7. C4 is more diffuse at the eastern edge of the transect, yet neither the Moyston or Pleasant Creek Faults deviate at depth in Figure 8, they likely either terminate at the Moho or propagate through it. As C4 is bound by the Moyston and Pleasant Creek Faults, the conductor will match the trend of the faults. C4 therefore likely extends beneath the Moho, hence fluids were derived from a mantle source; potentially the sub-continental lithospheric mantle (Griffin et al., 2013).

The mantle in Figure 7 is largely homogeneous, with a conductivity of $\sim$1 000 Ωm, no anomalies potentially related to subduction exist. Subduction related to the Lachlan

Orogen is >400 Ma, so despite being low angle initially, slab rollback and detachment may have occurred since (Royden, 1993). Subsequent to detachment, the conductive slab may have been recycled into the mantle, removing the anomalous zones from Figure 7. New mantle replacing the slab would not be anomalously conductive, hence the homogeneity.

Reconstructed geological history

Figure 2 shows the extensional and compressional history of the Tasmanides, and can be used to explain conductive anomalies within the crust. Current day Victoria will show more pronounced compression and deformation, as shortening continued for ∼80 Ma after Figure 2b. Source of the mafic to ultramafic ribbons in Figure 8b is shown in Figure 2. Mafic fragments were exhumed during extension, and at the onset of compression were imbricated and buttressed to the west against the andesite arc. As the crust was subducted, wedges of crust were: incorporated into the accretionary wedge, emplaced beneath the wedge, and interlayered with the resistive Cambrian pelitic layers.

The Escondida Fault occurs along the boundary between andesite and the low grade sediments, faulting exhumed the andesitic arc east of the Escondida Fault. Ribboning of the conductive mafic to ultramafic basalt and interlayering with the resistive low grade sediments and high grade pelitic layers can also be attributed to the Escondida Fault. Figure 8b shows interlayering east of the Escondida Fault but not to the west, so must be controlled by faulting.

The subducting slab present in Figure 2b may no longer exist, and hence is not seen in Figures 7 and 8. Further slab rollback may have occurred eventually causing the slab

to detach and be recycled, the mantle in this case is homogeneously resistive. Mafic wedges of oceanic crust emplaced above the Moho are still present however.

CONCLUSIONS

A 2D inversion of the MT data over the transition from the Delamerian Orogen to Lachlan Orogen imaged sub-horizontal conductors of 50-100 Ωm at 25-30 km, from which three sub-vertical conductors (C1, C2, C3) extended to the surface. C1 corresponds to the Escondida Fault, C2 the Moyston Fault, and C3 the Avoca Fault. The Moho is at ∼40 km, the mantle is homogeneous with a resistivity of ∼1 000 Ωm.

Ancient subducted mafic to ultramafic Proterozoic oceanic crust underwent serpentinisation, altering its conductivity. Magnetite mineralisation around grain boundaries formed during serpentinisation, and is the source of conductive anomalies. Conductive pathways associated with shear zones caused deformation and connectivity of magnetite. Interconnected magnetite within shear zones significantly increases conductivity, as conductivity depends more on interconnectivity, than volume percentage of magnetite. A homogeneous mantle does not preclude subduction. Slab rollback and detachment may have occurred after the Lachlan Orogen, causing the serpentinised slab to sink into, and be recycled by the mantle. Fluids post dating subduction, but not currently present, are likely from an exotic mantle source rather than crustally derived. Fluid source was determined by the Moyston and Pleasant Creek Faults, conduits which propagate through the Moho, and sourced fluids related to alteration from the mantle.

ACKNOWLEDGEMENTS

I would like to thank Graham Heinson, my supervisor, and Stephan Thiel, my co-supervisor for continued support and guidance through my thesis. The Geological Survey of Victoria, and specifically David Taylor and Phil Skladzien for correspondence and material. Thanks to the ASEG Research Foundation for financial support. Zara Dennis and Kate Robertson for past data from adjacent survey, and Kate specifically for contin-

ued discussion and help. Computer support came from Lars Krieger and Dennis Conway.

Thank you Goran, Alison, Kate, Paul and Olly for field work and support, and AuScope for allowing us to use the equipment. The University of Adelaide, School of Environmental and Earth Sciences for funding.

Also Thanks to Katie Howard and Ros King, the honour supervisors, for guidance throughout the year.

REFERENCES

Aivazpourporgou, S., Thiel, S., Hayman, P., Moresi, L. & Heinson, G. (2013). Results from long-period MT array in the Newer Volcanic Province, western Victoria, Australia, *ASEG Extended Abstracts* **2013**(1): 1–3.

Bahr, K. (1988). Interpretation of the magnetotelluric impedance tensor: regional induction and local telluric distortion, *Journal of Geophysics* **62**: 119–127.

Bibby, H. M., Caldwell, T. G. & Brown, C. (2005). Determinable and non-determinable parameters of galvanic distortion in magnetotellurics, *Geophysical Journal International* **163**(3): 915–930.

Box, G. E. P. & Draper, N. R. (1987). *Empirical model-building and response surfaces*, John Wiley and Sons.

Caglar, I. (2001). Electrical resistivity structure of the northwestern Anatolia and its tectonic implications for the Sakarya and Bornova zones, *Physics of the Earth and Planetary Interiors* **125**(14): 95 – 110.

Cagniard, L. (1953). Basic theory of the magneto-telluric method of geophysical prospecting, *Geophysics* **18**(3): 605–635.

Caldwell, T. G., Bibby, H. M. & Brown, C. (2004). The magnetotelluric phase tensor, *Geophysical Journal International* **158**(2): 457–469.

Cammarano, F., Goes, S., Vacher, P. & Giardini, D. (2003). Inferring upper-mantle temperatures from seismic velocities, *Physics of the Earth and Planetary Interiors* **138**(34): 197–222.

Cayley, R. A. (2011). Exotic crustal block accretion to the eastern Gondwanaland margin in the Late Cambrian Tasmania, the Selwyn Block, and implications for the Cambrian Silurian evolution of the Ross, Delamerian, and Lachlan orogens, *Gondwana Research* **19**(3): 628–649.

Cayley, R. A., Korsch, R. J., Moore, D. H., Costelloe, R. D., Nakamura, A., Willman, C. E., Rawling, T. J., Morand, V. J., Skladzien, P. B. & O'Shea, P. J. (2011). Crustal architecture of central Victoria: results from the 2006 deep crustal reflection seismic survey, *Australian Journal of Earth Sciences* **58**(2): 113–156.

Cayley, R., Korsch, R., Kennett, B., Skladzien, P., Jones, J., Morand, V., Gibson, G., Rawling, T. & Betts, P. (2011a). *Results of a deep seismic reflection imaging of the eastern Delamerian Orogen, South Australia and western Victoria, Australia*, GeoScience Department of Primary Industries, Victoria.

Chave, A. D. & Jones, A. G. (2012). *The magnetotellutic method theory and practice*, Vol. 1, Cambrisge University Press, Cambridge.

Chave, A. D. & Thomson, D. J. (2004). Bounded influence magnetotelluric response function estimation, *Geophysical Journal International* **157**(3): 988–1006.

Crawford, A., Cayley, R., Taylor, D., Morand, V., Gray, C., Kemp, A., Wohlt, K., VandenBerg, A., Moore, D., Maher, S., Direen, N., Edwards, J., Donaghy, A., Anderson, J. & Black (2003). *Neoproterozoic and Cambrian continental rifting, continentarc collision and post-collisional magmatism*, Geological Society of Australia.

Dennis, Z. R., Moore, D. H. & Cull, J. P. (2011b). A geological interpretation of the Echuca magnetotelluric survey, Victoria, *Australian Journal of Earth Sciences* **58**(6): 587–597.

Faul, U. H. & Jackson, I. (2005). The seismological signature of temperature and grain size variations in the upper mantle, *Earth and Planetary Science Letters* **234**(12): 119–134.

Ferguson, I., Epp, D., Saturino, T., Orellana, M., Craven, J. & Jones, A. G. (2015). Interpretation of resistivity and magnetic anomalies from the Fox River Sill, Trans Hudson Orogen, Canada.

Fergusson, C. L. (2003). Ordovician Silurian accretion tectonics of the Lachlan Fold Belt, southeastern Australia, *Australian Journal of Earth Sciences* **50**(4): 475–490.

Fergusson, C. L. (2010). Plate-driven extension and convergence along the East Gondwana active margin: late Silurian Middle-Devonian tectonics of the Lachlan Fold Belt, southeastern Australia, *Australian Journal of Earth Sciences* **57**(5): 627–649.

Foden, J., Elburg, M. A., Dougherty-Page, J. & Burtt, A. (2006). The timing and duration of the Delamerian Orogeny: Correlation with the Ross Orogen and implications for Gondwana assembly, *The Journal or Geology* **114**: 22.

Foster, D. A. & Gray, D. R. (2000). Evolution and Structure of the Lachlan Fold Belt (Orogen) of Eastern Australia, *Annual Review of Earth and Planetary Sciences* **28**(1): 47–80.

Foster, D. A., Gray, D. R. & Spaggiari, C. (2005). Timing of subduction and exhumation along the Cambrian East Gondwana margin, and the formation of Paleozoic backarc basins, *Geological Society of America Bulletin* **117**(1-2): 105–116.

Galanopoulos, D., Sakkas, V., Kosmatos, D. & Lagios, E. (2005). Geoelectric investigation of the Hellenic subduction zone using long period magnetotelluric data, *Tectonophysics* **409**(14): 73 – 84.

Graeber, F. M., Houseman, G. A. & Greenhalgh, S. A. (2002). Regional teleseismic tomography of the western Lachlan Orogen and the Newer Volcanic Province, southeast Australia, *Geophysical Journal International* **149**(2): 249–266.

Griffin, W. L., Begg, G. C. & O'Reilly, S. Y. (2013). Continental-root control on the genesis of magmatic ore deposits, *Nature Geoscience* **6**(11): 905–910.

Griffin, W. L., O'Reilly, S. Y., Afonso, J. C. & Begg, G. C. (2008). The composition and evolution of lithospheric mantle: a re-evaluation and its tectonic implications, *Journal of Petrology* **50**(7): 1185–1204.

Hyndman, R. D. & Shearer, P. M. (1989). Water in the lower continental crust: modelling magnetotelluric and seismic reflection results, *Geophysical Journal International* **98**(2): 343–365.

Hyndman, R., Vanyan, L., Marquis, G. & Law, L. (1993). The origin of electrically conductive lower continental crust: saline water or graphite?, *Physics of the Earth and Planetary Interiors* **81**(14): 325 – 345.

Jones, A. G. (1987). MT and reflection: an essential combination, *Geophysical Journal International* **89**(1): 7–18.

Jones, A. G. (1993). Electromagnetic images of modern and ancient subduction zones, *Tectonophysics* **219**(13): 29–45.

Kawano, S., Yoshino, T. & Katayama, I. (2012). Electrical conductivity of magnetite-bearing serpentinite during shear deformation, *Geophysical Research Letters* **39**(20): n/a–n/a.

Korsch, R. J., Barton, T. J., Gray, D. R., Owen, A. J. & Foster, D. A. (2002). Geological interpretation of a deep seismic-reflection transect across the boundary between the Delamerian and Lachlan Orogens, in the vicinity of the Grampians, western Victoria, *Australian Journal of Earth Sciences* **49**(6): 1057–1075.

Miller, J. M., Phillips, D., Wilson, C. J. L. & Dugdale, L. J. (2005). Evolution of a reworked orogenic zone: The boundary between the Delamerian and Lachlan Fold Belts, southeastern Australia, *Australian Journal of Earth Sciences* **52**(6): 921–940.

Myer, D., Constable, S. & Key, K. (2013). Magnetotelluric evidence for layered mafic intrusions beneath the Vøring and Exmouth rifted margins, *Physics of the Earth and Planetary Interiors* **220**(0): 1 – 10.

Parasnis, D. S. (1956). The electrical resistivity of some sulphide and oxide minerals and their ores, *Geophysical Prospecting* **4**(3): 249–278.

Phillips, G., Miller, J. M. & Wilson, C. J. L. (2002). Structural and metamorphic evolution of the Moornambool Metamorphic Complex, western Lachlan Fold Belt, southeastern Australia, *Australian Journal of Earth Sciences* **49**(5): 891–913.

Rawlinson, N. & Fishwick, S. (2011). Seismic structure of the southeast Australian lithosphere from surface and body wave tomography, *Tectonophysics* **572**(0): 111–122.

Rawlinson, N., Kennett, B. L. N., Vanacore, E., Glen, R. A. & Fishwick, S. (2010). The structure of the upper mantle beneath the Delamerian and Lachlan Orogens from simultaneous inversion of multiple teleseismic datasets, *Gondwana Research* **19**(3): 788–799.

Reynard, B., Mibe, K. & de Moortle, B. V. (2011). Electrical conductivity of the serpentinised mantle and fluid flow in subduction zones, *Earth and Planetary Science Letters* **307**(34): 387 – 394.

Robertson, K., Taylor, D., Thiel, S. & Heinson, G. (2014). Magnetotelluric evidence for serpentinisation in a Cambrian subduction zone beneath the Delamerian Orogen, southeast Australia, *Gondwana Research* .

Royden, L. H. (1993). Evolution of retreating subduction boundaries formed during continental collision, *Tectonics* **12**(3): 629–638.

Shalivahan & Bhattacharya, B. B. (2002). How remote can the far remote reference site for magnetotelluric measurements be?, *Journal of Geophysical Research: Solid Earth* **107**(B6): ETG 1–1–ETG 1–7.

Simpson, F. & Bahr, K. (2005). *Practical Magnetotellurics*, Vol. 1, Cambridge University Press.

Smith, R. J. & Frankcombe, K. (2006). Role of geophysical methods applied to mapping mineral systems under the Murray Basin cover, *Australian Journal of Earth Sciences* **53**(5): 767–781.

Soesoo, A., Bons, P. D., Gray, D. R. & Foster, D. A. (1997). Divergent double subduction: Tectonic and petrologic consequences, *Geology* **25**(8): 755–758.

Spaggiari, C. V., Gray, D. R. & Foster, D. A. (2004). Lachlan Orogen subduction accretion systematics revisited, *Australian Journal of Earth Sciences* **51**(4): 549–553.

Spaggiari, C. V., Gray, D. R., Foster, D. A. & Fanning, C. M. (2002). Occurrence and significance of blueschist in the southern Lachlan Orogen, *Australian Journal of Earth Sciences* **49**(2): 255–269.

Spaggiari, C. V., Gray, D. R., Foster, D. A. & McKnight, S. (2003). Evolution of the boundary between the western and central Lachlan Orogen: implications for Tasmanide tectonics, *Australian Journal of Earth Sciences* **50**(5): 725 – 749.

Squire, R. J. & Miller, J. M. L. (2003). Synchronous compression and extension in East Gondwana: tectonic controls on world-class gold deposits at 440 Ma, *Geology* **31**(12): 1073–1076.

Stesky, R. M. & Brace, W. F. (1973). Electrical conductivity of serpentinized rocks to 6 kilobars, *Journal of Geophysical Research* **78**(32): 7614–7621.

Thiel, S. (2008). *Modelling and inversion of magnetotelluric data for 2-D and 3-D lithospheric structure, with application to obducted and subducted terranes*, PhD thesis.

Tikhonov, A. N. (1950). On determining electrical characteristics of the deep layers of the Earth's crust, *Doklady Akademia Nauk* **73**: 295–297.

Unsworth, M. (2010). Magnetotelluric studies of active continent continent collisions, *Surveys in Geophysics* **31**(2): 137–161.

VandenBerg, A. H. M. (1976). The Tasman Fold Belt in Victoria, *Technical report*, Mines Department Victoria.

VandenBerg, A., Willman, C., Maher, S., Simons, B., Cayley, R., Taylor, D., Morand, V., Moore, D. & Radojkovic, A. (2000). *The Tasman Fold Belt System in Victoria*, Geological Survey of Victoria Special Publication.

Willman, C. E., Korsch, R. J., Moore, D. H., Cayley, R. A., Lisitsin, V. A., Rawling, T. J., Morand, V. J. & OShea, P. J. (2010). Crustal-scale fluid pathways and source rocks in the victorian gold province, Australia: Insights from deep seismic reflection profiles, *Economic Geology* **105**(5): 895–915.

Worzewski, T., Jegen, M., Kopp, H., Brasse, H. & Castillo, W. T. (2010). Magnetotelluric image of the fluid cycle in the Costa Rican subduction zone, *Nature Geoscience* **4**(2): 108–111.

APPENDIX A: QUALITY ASSESSMENT

Assessing and classing data quality after each stage of creating edi's.

Station	Ex/By Correlation	Ey/Bx Correlation	No RR	With RR	Dec100
DLT01	Y	Y	Good	Good	Good
DLT02	Y	Y	Average	Average	Poor
DLT03	Y	N	Good	Good	Good
DLT04	Y	Y	Poor	Average	Poor
DLT05	Y	Y	Average	Average	Good
DLT06	N	Y	Good	Good	Good
DLT07	N	Y	Poor	Average	Average
DLT08	N	Y	Average	Average	Average
DLT09	Y	Y	Good	Good	Good
DLT10	Y	N	Average	Average	Good
DLT11	Y	N	Poor	Poor	Poor
DLT12	N	Y	Average	Average	Average
DLT13	Y	Y	Poor	Average	Unusable
DLT14	Y	Y	Poor	Average	Average
DLT15	N	N	Poor	Average	Good
DLT16	N	Y	Average	Average	Average
DLT17	Y	Y	Poor	Good	Good
DLT18	Y	Y	Good	Good	Average
DLT19	N	N	Poor	Good	Average
DLT20	N/A	N/A	Poor	Poor	Average
DLT21	N	Y	Poor	Poor	Poor
DLT22	N/A	N/A	Poor	Poor	Poor
DLT23	Y	Y	Poor	N/A	N/A
DLT24	Y	N	Good	Good	Average
DLT25	Y	Y	Average	Average	Average
DLT26	N	N	Average	Average	Average
DLT27	N	Y	Poor	Poor	Poor
DLT28	Y	Y	Poor	Poor	Poor

DLT29a	N/A	N/A	Poor	Poor	Average
DLT29	N	Y	Average	Good	Poor
DLT30a	Y	Y	Poor	Good	Poor
DLT30	Y	Y	Unusable	Poor	Unusable
DLT31a	N	N	Good	Good	Good
DLT31	N	Y	N/A	Good	Good
DTL32a	Y	N	Average	Good	Good
DLT32	Y	Y	Good	Average	Good
DLT33a	N	N	Average	Average	Good
DLT33	Y	Y	Poor	Poor	Poor
DLT34a	N	N	Good	Good	Poor
DLT34	Y	N	Poor	Unusable	Unusable
DLT35a	N/A	N/A	Unusable	Good	Good
DLT35	Y	Y	Average	Good	Good
DLT36a	N/A	N/A	Unusable	Unusable	Good
DLT36	N/A	N/A	Poor	Good	Good